#24-067
2024 AFS Proceedings ©American Foundry Society

Cast Metal-Ceramic Lattice Structures for Lightweight Energy Absorbing and/or Penetration Resistant Structures

Alan P. Druschitz
Virginia Tech, Materials Science and Engineering, Blacksburg, Virginia, USA

Manuel Umanzor
Corning, Manufacturing Technology and Engineering, Corning, New York, USA

ABSTRACT

Cast metal-ceramic lattice structures were produced using 3D printed sand molds from a variety of metals and ceramic/hard metal tiles. The lattice structure properties (deformation in compression and penetration resistance) were determined and then models were developed to allow optimization of these structures and to allow designers to develop lattice structures tailored to specific applications. Cast metal-ceramic lattice structures were demonstrated to 1) reduce the weight of a component (since the majority of the structure is open space) while maintaining as good or better penetration resistance and 2) have superior penetration resistance compared to a solid piece of metal by combining an appropriate ceramic or hard metal tile within the lattice structure. 3D printed sand molding is the most economical way to produce large lattice structures and 3D printed sand molds with provisions to incorporate tiles is currently the only method that can produce lattice structure with embedded tiles.

Keywords: lattice structure, 3D printed sand, metals, ceramics, penetration resistance, cast

INTRODUCTION

An excellent review of the characteristics of cellular solids (honeycombs, sponges, bones) has been published by Gibson and Ashby.[1] Cellular solids are generally classified as having either random or periodic structures and are candidates for lightweight, structural applications.[1,2] In this study, the cellular solid was a network of trusses (commonly called a lattice structure) that was designed to absorb energy by plastically deforming and collapsing during compressive loading.[1,3] Two deformation mechanisms (bending and stretching) are possible. Deformation by stretching typically results in the highest strength-to-weight ratios, but, deformation by bending is most commonly observed.[4]

Structures with randomly oriented and randomly sized porosity can be manufactured by foaming molten metal and structures with well-defined porosity can be manufactured by additive manufacturing.[5-7] Metalcasting approaches have shown excellent promise for the manufacture of large lattice structures. Examples of metalcasting approaches are 3D printing disposable patterns for investment casting[8] and 3D printing sand molds for gravity pouring.[9] A356 alloy castings made with 3D printed sand molds have shown the identical mechanical properties as castings made in traditional no-bake sand molds.[9] The dimensional accuracy of 3D printed sand molds are superior to green sand molds.[10] For lattice structures with round trusses, a truss diameter of about 2.5 mm is a physical limitation for some sand/binder combination (silica sand/furan binder) due to difficulties with removing unbonded sand from the 3D printed molds.[11,12] Direct additive manufacturing technologies, such as laser powder bed fusion, is a competitor to sand casting but laser powder bed fusion is limited by defects caused by extremely high solidification and cooling rates, preferred crystallographic orientation, lack of fusion, cracking, and high residual stresses.[13-15] Another benefit of casting combined with 3D printed sand molds is the ability to incorporate objects within the sand mold that are encapsulated by the metal during casting. Metalcasting using 3D printed sand molds is the approach that we used to produce cast metal lattice structures with or without encapsulated hard ceramic or hard metal tiles. Hard ceramic or hard metal tiles were added to the cast metal structures if penetration resistance was desired.

For this project, castings were produced from six metal alloys: A356 aluminum alloy, F356 aluminum alloy, A206 alloy plus 1% TiC nanoparticles, high hardness steel, ultra-high hardness steel, and Fe30Mn4Al1Si0.9C austenitic steel. Aluminum alloys have low density plus reasonable strength, which gives them a good strength-to-weight ratio. Steel alloys are much stronger, much harder, and have a higher density compared to aluminum alloys. Assuming that energy absorbed during deformation can be represented by the area under the load versus displacement curve, ductile steel alloys would be expected to absorb more energy compared to aluminum alloys. Also, since penetration resistance is loosely related to hardness, the higher hardness steel structures would be

expected to have better penetration resistance. However, steel structures will be heavier. Two ceramic materials (pressureless sintered SiC and pressureless sintered SiC/B_4C composite), one hard metal (white cast iron), and integrally cast steel were used for the tile materials to improve penetration resistance. The ceramic materials chosen for this study had low density, high hardness, and low cost. By using pressureless sintered ceramics, tooling and processing is inexpensive so any desired shape can be obtained at a reasonable cost. White cast iron was also used as a tile material since it is inexpensive, has high hardness (although not as hard as a ceramic), can be cast to any desired thickness, and can be waterjet cut to any desired shape. Therefore, white cast iron is a lower cost alternative to ceramics but white cast iron has a higher density than ceramics, which results in a heavier final product. Finally, for high hardness steel, the cast steel alloy was used to integrally cast tiles of the same material, which is the lowest cost solution. Five lattice structure designs (octet truss, auxetic truss, Kelvin foam, circular octet, and face centered truss) were investigated since each design has unique properties.

EXPERIMENTAL PROCEDURE

The octet truss was chosen as the first lattice structure to evaluate. Mold designs with and without provisions for tiles were developed using CAD. Only the core that would produce the lattice structure and the “box” that would contain the lattice core were designed to be 3D printed in silica sand. The drag mold, downsprue(s), runner system, and pouring basin were produced using conventional air-set molding techniques. Since we had prior experience with designing 3D printed sand lattice cores, the focus of this project was to make the core sufficiently robust so that lattice castings could be produced in commercial foundries.

Ultimately, a decision was made to incorporate three rows of tiles. Three rows of tiles were desirable because there was no pathway through the casting without hitting a tile and the tiles did not touch each other and thus create a plane of weakness. This required that the core be two pieces. Provisions were added to the cores to ensure proper alignment, “pins” to hold the ceramic or hard metal tiles in position, and locators to prevent the cores from floating during mold filling.

For the majority of the project, the 3D printed sand cores were produced using furan binder and silica sand. For the final year of the project, 3D printed sand cores were produced using phenolic urethane binder and silica sand or furan binder and silica sand. It took three iterations to reach the final mold design.

The first mold design had provisions for only six hexagonal tiles that were 30 mm across flats; two 4 mm thick tiles, two 6 mm thick tiles, and two 8 mm thick. This mold had a 3D printed core that contained the lattice structure, had provisions for locating the tiles, and had provisions to prevent the core from floating. The 3D printed core was 225 mm by 225 mm by 50 mm thick. A 3D printed cover that had provisions to prevent the tiles from floating was placed on top of the core and the assembled core package was placed on a conventional molded drag with two downsprues and a pouring basin that fed both downsprues.

The 3D printed sand cores and the completely assembled mold are shown in Figure 1. A complete casting with gating is shown in Figure 2.

The third mold design had provisions for thirty-nine, 6 mm thick tiles. This mold had a two-piece, 3D printed sand core that contained the lattice structure, provisions for locating the tiles, provisions for preventing the core from floating, and provisions for locating the individual core pieces in top and bottom covers to ensure correct assembly. The cores were placed in 3D printed bottom and top covers and the assembled core package was placed on a conventionally molded drag with two downsprues and a pouring basin that fed both downsprues. The assembly sequence for this 3D printed core package is shown in Figure 3.

Lattice castings were produced in six metal alloys: A356 aluminum alloy, F356 aluminum alloy, A206 alloy plus 1% TiC nanoparticles, high hardness steel, ultra-high hardness steel, and Fe30Mn4Al1Si0.9C austenitic steel. Two ceramic materials (pressureless sintered SiC and pressureless sintered SiC/B_4C composite), one hard metal (white cast iron), and integrally cast steel were used for the tile materials to improve penetration resistance. The chemistries of the metals cast are listed in Tables 1-4.

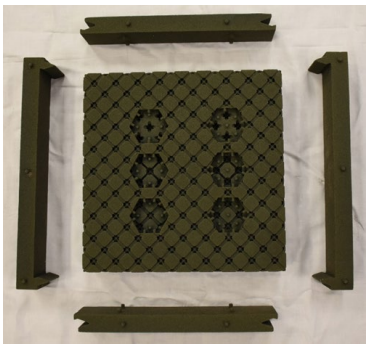
core with sides

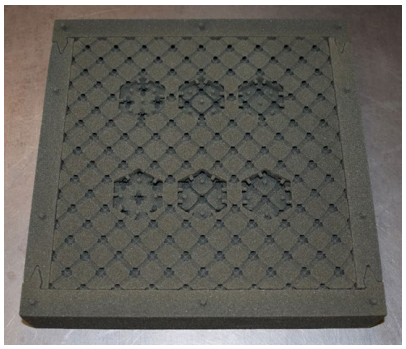
core with tile locators

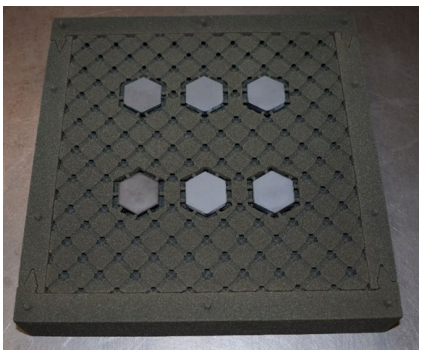
core with six tiles in place

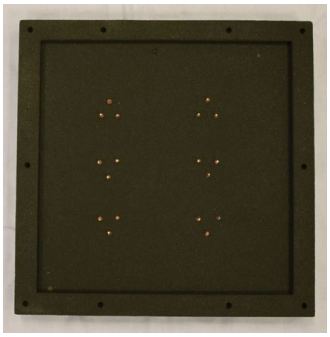
top with tile locator pins

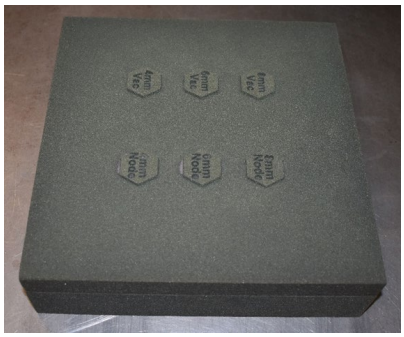
assembled core package


completed mold

Figure 1. Initial 3D printed sand mold for lattice castings containing six tiles of varying thickness.

Figure 2. Complete lattice casting with six embedded tiles of varying thickness.

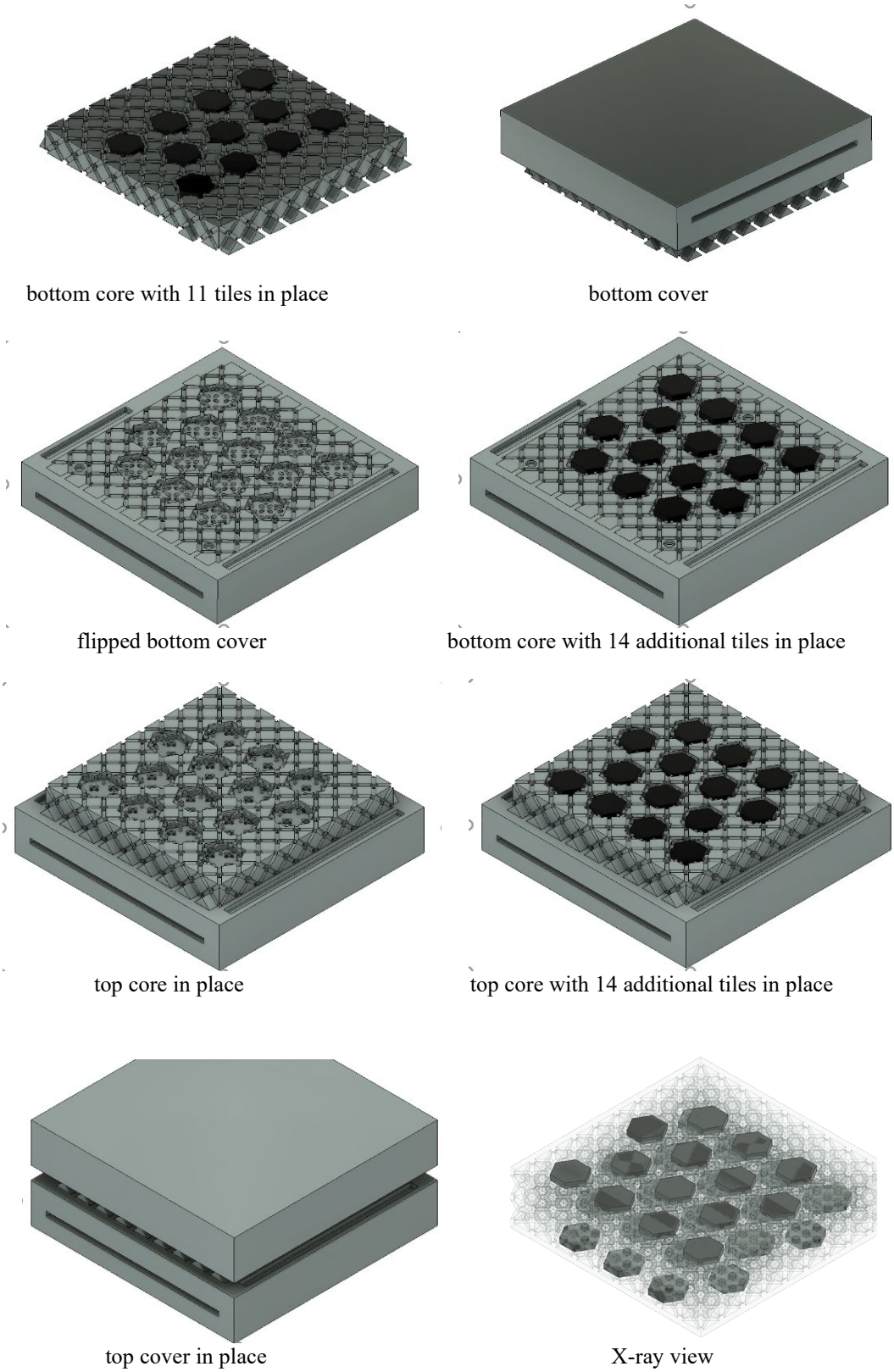

Figure 3. The 3D printed core package assembly sequence for producing a lattice structure mold with thirty-nine (39) embedded tiles.

Table 1. A356 Aluminum Alloy Casting Compositions

	Average Composition, wt%								
Cast Date	Si	Mg	Fe	Ti	Cu	Mn	Zn	others	Al
Spec[16]	6.5-7.5	0.25-0.45	<0.20	<0.20	<0.20	<0.10	<0.10	<0.05	bal
9/26/18	6.8	0.33	0.15	0.14	0.01	<0.10	<0.10	<0.05	bal
10/5/18	7.1	0.33	0.15	0.17	0.04	<0.10	<0.10	<0.05	bal
10/25/18	6.8	0.32	0.11	0.14	0.05	<0.10	<0.10	<0.05	bal
10/31/19	6.6	0.30	0.12	0.14	0.02	<0.10	<0.10	<0.05	bal
10/31/19	6.6	0.28	0.11	0.14	0.03	<0.10	<0.10	<0.05	bal
10/31/19	6.4	0.29	0.11	0.14	0.02	<0.10	<0.10	<0.05	bal
3/1/19	6.3	0.33	0.10	0.13	0.01	<0.10	<0.10	<0.05	bal
3/6/19	6.5	0.39	0.10	0.14	0.03	<0.10	<0.10	<0.05	bal
4/12/19	6.9	0.29	0.12	0.15	0.15	<0.10	<0.10	<0.05	bal
4/12/19	6.8	0.30	0.11	0.14	0.06	<0.10	<0.10	<0.05	bal
12/8/21	7.0	0.36	0.10	0.14	0.03	<0.10	<0.10	<0.05	bal
12/8/21	6.9	0.36	0.09	0.15	0.02	<0.10	<0.10	<0.05	bal

Table 2. F356 Aluminum Alloy Casting Compositions

	Average Composition, wt%								
Cast Date	Si	Mg	Fe	Ti	Cu	Mn	Zn	others	Al
Spec[16]	6.5-7.5	0.17-0.25	<0.20	0.04-0.20	<0.20	<0.10	<0.10	<0.05	bal
11/14/19	7.0	0.21	0.05	0.04	0.05	0.006	<0.002	<0.05	bal
2/26/20	6.9	0.21	0.08	0.04	0.07	0.005	<0.002	<0.05	bal
9/24/20	7.2	0.21	0.06	0.02	0.04	0.002	<0.002	<0.05	bal
8/26/21	7.5	0.20	0.03	0.06	0.04	0.002	<0.002	<0.05	bal
10/27/21	7.2	0.21	0.03	0.06	0.02	<0.002	<0.002	<0.05	bal

Table 3. High and Ultra-High Hardness Steel Alloy Casting Compositions

	Average Composition, wt%									
Alloy	C	Ni	Cr	Si	Mn	Mo	P	S	Al	Fe
15N20	0.70	2.06	0.07	0.44	0.73	0.10	0.031	0.016	0.09	bal
4365	0.65	1.82	0.82	0.41	0.90	0.25	0.014	0.011	0.12	bal

Table 4. Fe30Mn(4-9)Al Steel Alloy Casting Compositions

	Average Composition, wt%						
	Mn	Al	Si	C	Mo	S	Fe
Target	30	4-9	1	0.9	0.5	<0.020	bal
4/17/19 – ICP/Leco	31.5	4.7	1.1	1.1	0.5	0.014	bal
1/13/20 - Leco				1.0		0.010	bal
8/10/20 - EDS	28.9	4.9	0.8	nd*	0.8	nd	bal
1/20/21 - EDS	30.7	8.8	0.8	nd	0.9	nd	bal
12/6/21 - EDS	29.8	4.1	0.7	nd	0.5	nd	bal
9/16/22 – ICP/Leco	30.0	4.25	1.15	0.94	nd	0.011	bal
12/1/2022							

* not determined

Penetration resistance was determined by a commercial test lab.[17] If a penetrator went completely through the lattice structure, residual velocity was measured. This allowed us to develop a penetration model that could predict the performance of the cast aluminum alloy lattice structures. A variety of penetrators were evaluated: 0.30 cal APM2, 7.62 x 51 full metal jacket M80 ball rounds, 0.50 caliber APM2, 0.50 caliber fragment simulated projectiles, and 20 mm fragment simulated projectiles. A commercial, explicit simulation, software package,[18] was used to model penetration resistance for aluminum lattice structures with and without tiles. The effects of the strength of the tile/matrix interface and tile compressive residual stresses were also modeled.

Small, 50 mm x 50 mm x 75 mm, lattice structure castings were produced for compression testing. The mold design for the 50 mm x 50 mm x 75 mm lattice structure castings is shown in Figure 4 and two 50 mm x 50 mm x 75 mm, lattice structure castings are shown in Figure 5.

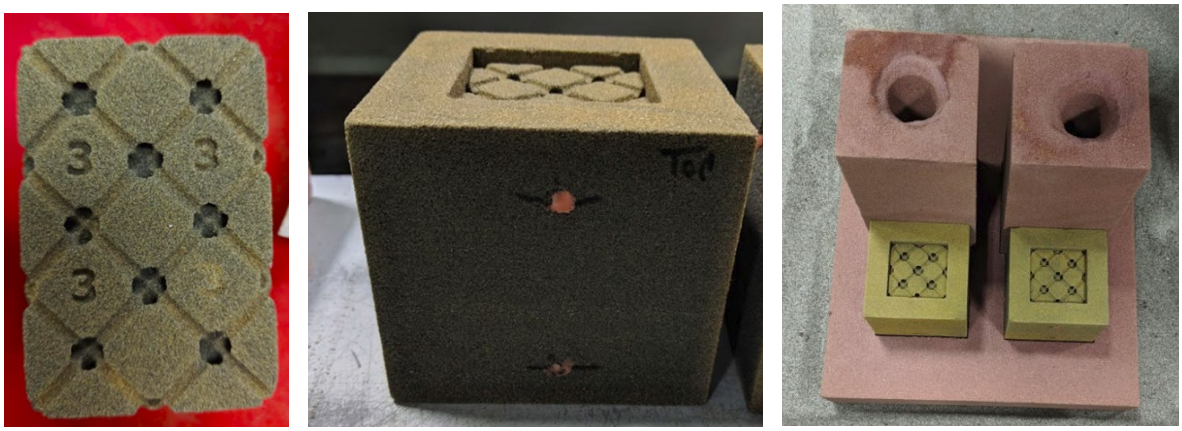

core (3 mm dia. trusses) core in sleeve completed mold

Figure 4. 3D printed mold design for small, 50 mm x 50 mm x 75 mm, lattice structures for compression testing. The "completed" mold is missing the lattice sleeve covers.

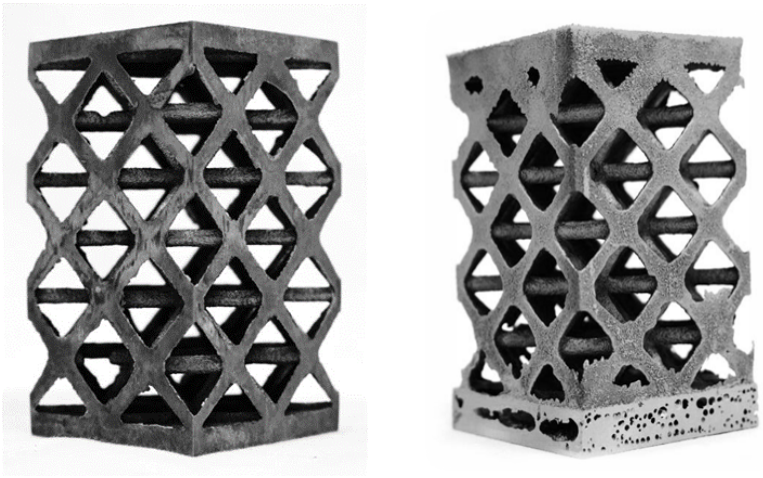

3.0 mm dia trusses, A356 alloy 4.0 mm dia trusses, steel

Figure 5. Two lattice structure castings (50 mm x 50 mm x 75 mm); one with 3.0 mm diameter trusses cast in A356 aluminum alloy and one with 4.0 diameter trusses cast in steel.

Deformation in compression was determined using the small, 50 mm x 50 mm x 75 mm tall, lattice structures and a tensile/compression machine at a slow crosshead speed (1 mm per minute). For these tests, performance was determined by the maximum load, the load at the onset of truss fracture, and the energy absorbed at the onset of densification (the area under the load versus displacement curve).

A commercial casting process simulation software package,[19] was used to model mold filling and solidification. Predicted porosity for lattice castings was compared to the actual porosity and the agreement was good. A commercial computational materials modeling software package,[20] was used to predict the physical properties needed for modeling Fe30Mn4Al1Si0.9C.

The mechanical properties of the metals investigated were determined using industry standard test procedures. The Fe30Mn4Al1Si0.9C steel investigated was previously considered not heat treatable, however, we determined that this steel could be heat treated but the change in mechanical properties was small.

RESULTS AND DISCUSSION

METAL-CERAMIC LATTICE STRUCTURES

Two basic mold designs were developed. One mold design did not have provisions for embedding tiles and the other mold design did have provisions for embedding tiles. The mold design with no tiles could be used for energy absorbing applications, such as vehicle crush zones, earthquake resistant building supports, blast resistant doors, etc. The mold design with tiles was designed to absorb energy and resist penetration. The lattice unit cell dimensions were chosen to be 25 mm x 25 mm x 25 mm (1" x 1" x 1"). These dimensions were chosen so that structures could be easily built by repeating the unit cell in the x, y, and z directions.

Since lattice castings with dimensions of 150 mm x 150 mm x 150 mm thick had been previously produced, the first casting size for this project was 225 mm x 225 mm x 50 mm thick with the addition of 6 mm thick front and back faces. The first castings with tiles had provisions for six tiles; two 4 mm thick tiles, two 6 mm thick tiles, and two 8 mm thick tiles. These castings were used to determine the effect of tile thickness on penetration resistance. A356 aluminum alloy was chosen as the first alloy to cast due to its low cost, good fluidity, and good resistance to hot tearing. The cast metal and tile combinations produced throughout this project are summarized in Table 5 for lattice castings with no tiles and Table 6 for lattice castings with only six tiles.

Table 5. Cast Lattice Structures (225 mm x 225 mm x 62 mm) with No Tiles

Cast Metal	Truss Diameter (mm)	Open Volume (%)	Casting Weight (lbs)	Number of Castings Produced
A356 aluminum	3	84	6.3-6.4	2
	3.5			1
	4	74	7.8	6
A206*	4	74	9.2	1
Fe30Mn4Al1Si0.9C	3	84	15.4	1
	3.5			1
	4	74	19.2	1
Fe30Mn9Al1Si0.9C	3.5		15.9	1
	4	74	16.9	1

* A206 alloy with 1% TiC nanoparticles cast at Eck Industries, Manitowoc, WI

Table 6. Cast Metal & Tile Combinations Produced with Six Tiles

Cast Metal	Truss Diameter (mm)	Tile Material	Number of Castings Produced
A356 aluminum	4	SiC	2
	4	white cast iron	1
Fe30Mn4Al1Si0.9C	4	SiC	1
Fe30Mn9Al1Si0.9C	4	CP-Ti & SiC	1

A new second lattice casting design that would have no pathway through the casting without hitting a tile was also designed. This 225 mm x 225 mm x 62 mm thick casting design contained thirty-nine (39) tiles. The mold design was much more complicated since the tiles were spread over three levels to produce a structure with multi hit capability and so that a plane of weakness would not be created.

This mold design had a two-piece 3D printed sand core, top cover, and bottom cover. The cast metal and tile combinations produced are summarized in Table 7.

Table 7. Cast Metal & Tile Combinations for Lattice Castings (225 mm x 225 mm x 62 mm) with 39 6-mm Thick Tiles

Cast Metal	Truss Diameter (mm)	Tile Material	Casting Weight (lbs)	Number of Castings Produced
A356 aluminum	4	SiC	10.0	2
	4	B_4C/SiC iron		2
	4	white cast iron	11.4	2
A206*	4	B_4C/SiC	10.0	1
Fe30Mn4Al1Si0.9C	4	white cast iron	22.6-24.3	4
15N20 steel	4	15N20	27.9	1
4365 steel	4	4365 steel	25.7	1

* A206 alloy with 1% TiC nanoparticles cast at Eck Industries, Manitowoc, Wisconsin

MATERIAL PROPERTY DATABASE

The mechanical properties of the metals investigated were determined using industry standard test procedures. The Fe30Mn4Al1Si0.9C steel investigated was previously considered not heat treatable. It was determined that this steel could be heat treated but the change in mechanical properties was small. The A356 and F356 alloys were solution treated at 540C (1,004F) for 8 hours, warm water quenched, naturally aged at room temperature for 24 hours, and then artificially aged at 154C (309F) for 3-4 hours. Tensile samples were sectioned from separately cast Y-blocks. There was only one sample per test condition unless otherwise noted. The mechanical and physical properties determined for the materials investigated in this study are listed in Tables 8-11.

Table 8. Measured Compressive Properties for Cast Metals Investigated

Cast Metal	0.2% YS (MPa)	UCS (MPa)	Compression at Fracture (%)	Elastic Modulus (GPa)
A356 aluminum – 154°C for 3.5 hr.	196	562	>36	76
F356 aluminum – 154°C for 3.5 hr.	130			70
Fe30Mn4Al1Si0.9C – as-cast (3 tests)	371 +/- 8	>1160	>27	141 +/- 6

Table 9. Measured Tensile Properties For Cast Metals Investigated

Cast Metal	0.2% YS (MPa)	UTS (MPa)	Elongation at Fracture (%)	Elastic Modulus (GPa)
A356 aluminum – 154C/309F for 3 hr.	140	203	3.6	80
A356 aluminum – 154C/309F for 4 hr.	161	216	2.8	86
F356 aluminum – 154C/309F for 3.5	119	185	4.1	63
Fe30Mn4Al1Si0.9C – as-cast (2 tests)	391 +/- 3	681 +/- 19	42 +/- 6	153 +/- 10

Table 10. Measured Charpy V-notch Impact Strength at -40°C for Cast Metals Investigated

Cast Metal	Charpy V-notch impact strength at -40°C (joules)
A356 aluminum – 154C/309F for 3.5 hr.	3.2 +/- 0.6 (3 tests)
F356 aluminum – 154C/309F for 3.5 hr.	9.5 +/- 1.1 (3 tests)
Fe30Mn4Al1Si0.9C – as-cast, batch 1	71 +/- 10 (3 tests)
Fe30Mn4Al1Si0.9C – as-cast, batch 2	51 +/- 7 (4 tests)

Table 11. Measured Physical Properties for Cast Metals Investigated

Cast Metal	Density (g/cm^3)	Liquidus C/F	Solidus or Eutectic C/F	α to γ transformation during heating (C/F)
A356 aluminum	2.67	614-617C / 1137-1143F	560-573C / 1040-1063F	-----
F356 aluminum	2.65	612-613C / 1134-1135F	571-575C / 1060-1067F	-----
Fe30Mn4Al1Si0.9C	6.97-7.06	1330C (calculated) / 2426F	1267C (calculated) / 2313F	-----
Fe30Mn9Al1Si0.9C	6.60	1344-1348C / 2451-2458F	1319-1322C / 2406-2412F	-----
15N20 steel		1468C / 2674F	1371C / 2500F	719C / 1326F
4365 steel		1471C / 2680F	1381C / 2518F	732C / 1330F

LATTICE STRUCTURE MECHANICAL PROPERTIES

Deformation in compression was determined using small (50 mm x 50 mm x 75 mm tall) octet truss lattice structures. These structures were deformed using a tensile/compression machine at a slow crosshead speed (1 mm per minute). For these tests, performance was determined by the energy absorbed (the area under the load versus displacement curve) and the onset of truss failure. It was determined that material ductility was the most important factor in determining performance. The A356 and F356 alloys were solution treated at 540C (1004F) for 8 hours, warm water quenched, naturally aged at room temperature for 24 hours, and then artificially aged at 154C (309F) for 2-5 hours. The tensile properties of A356 aluminum alloy and the lattice compression test results for 4 mm diameter trusses are listed in Table 12. There was only one sample per test condition. The octet truss lattice structure design was subsequently enhanced by adjusting the diameter of trusses, Figure 6, and the radius of the fillet at the truss nodes, Figure 7. A comparison of the "standard" and "enhanced" lattice compression test results are listed in Table 13.

Table 12. Tensile Properties of A356 Al alloy and Standard Lattice Structure Compression Test Results for 4-mm diameter trusses

	Round Bar Tensile Tests		Lattice Compression Tests		
Artificial Aging Time (hrs.)	Yield Strength (MPa)	Elongation at Fracture (%)	Maximum Load (kN)	Displacement at the onset of Densification (mm)	Energy Absorbed up to the onset of Densification (joules)
2	147	3.2	56.9	17.5	682
3	141	3.8	52.7	16.7	514
4	162	3.3	63.4	11.7	458
5	185	1.3	62.9	11.8	420

Table 13. Comparison of "Standard" and "Enhanced" Lattice Compression Test Results. The Al Alloy Aging Time at 154C (309F) was 4 Hr

	Area Under the Curve (kN*mm)		
Material & Lattice Design	@ first truss fracture	@ maximum load	Total
A356 Standard	127	181	458
A356 Enhanced	345	212	>503
F356 Enhanced	233	124	>477

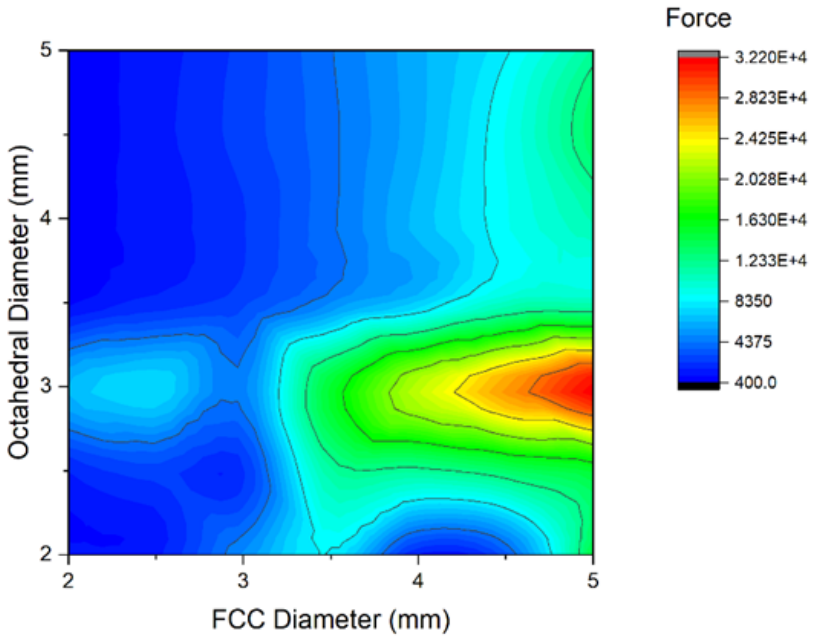

Figure 6. Effect of the octet truss diameter.

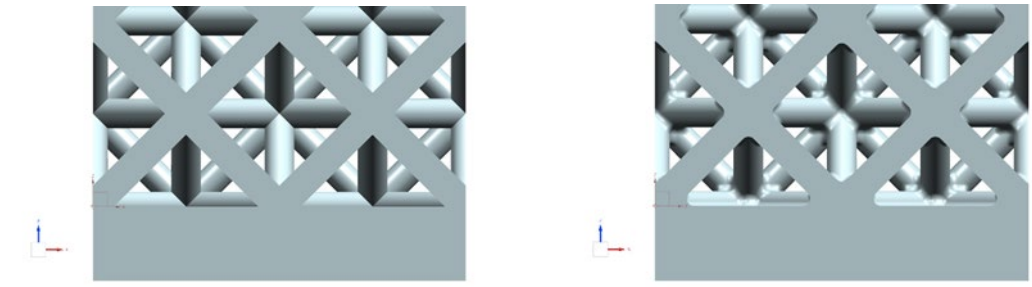

Octet truss with no fillet radius Octet truss with fillet radius

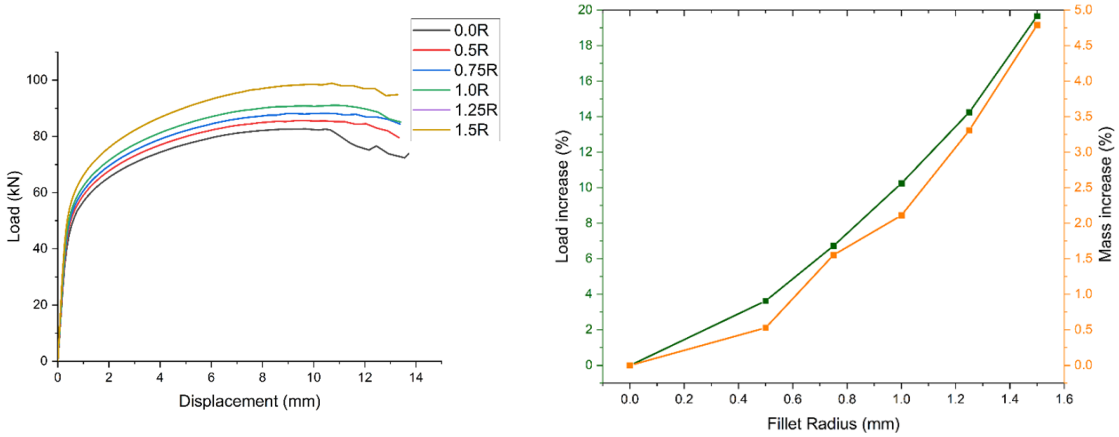

Figure 7. Effect of the fillet radius at the octet truss node. A 20% increase in peak load would only result in a 5% increase in weight.

Five lattice structure designs (octet truss, auxetic truss, Kelvin foam, circular octet, and face centered truss) were modeled. The auxetic truss was predicted to absorb the most energy but was also the most difficult to produce. The octet truss was determined to have the best combination of energy absorption and ease of production. The final model was able to satisfactorily predict the linear region, yield, and truss fracture during deformation in compression. The "bedding-in" phenomena for lattice structures was not captured in the model. The various lattice designs evaluated are shown in Figure 8 and a comparison of the specific absorbed energy (energy absorbed/mass) is shown in Figure 9.

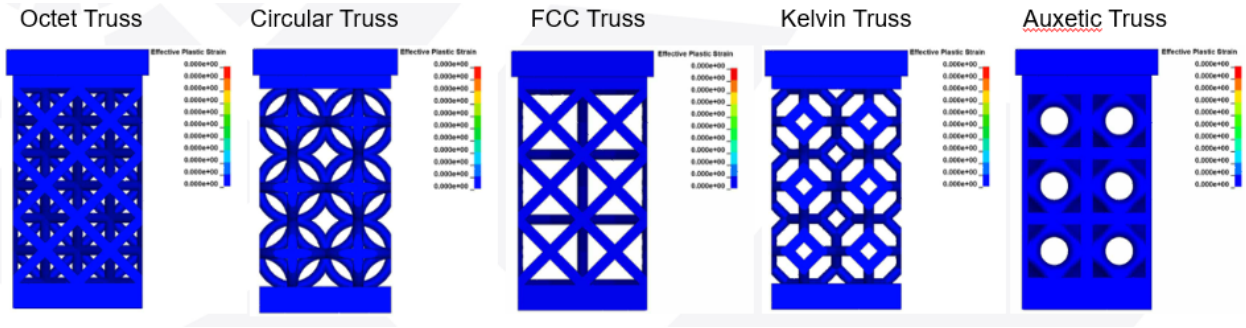

Figure 8. The five lattice designs evaluated.

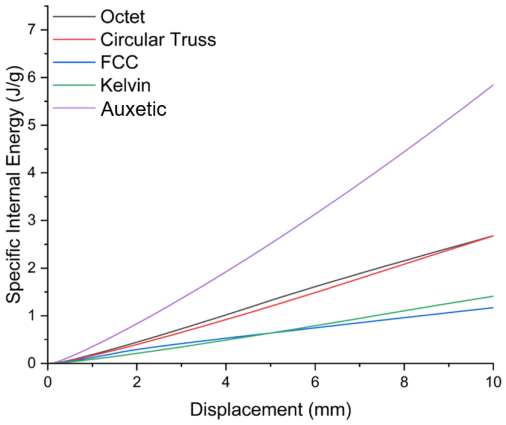

Figure 9. Specific absorbed energy (energy absorbed/mass) for the five lattice designs evaluated.

PENETRATION RESISTANCE

Throughout this investigation, a variety of penetrators were evaluated: 0.30 cal APM2, 7.62 x 51 full metal jacket M80 ball rounds, 0.50 caliber APM2, 0.50 caliber fragment simulated projectiles, and 20 mm fragment simulated projectiles. If a penetrator went completely through the lattice structure, residual velocity was measured.

Penetration resistance testing of A356 aluminum alloy lattice castings with embedded tiles showed three phenomena: 1) no projectile penetration, 2) full projectile penetration, and 3) projectile plus tile completely exiting the structure. An example of an aluminum lattice structure with SiC tiles that prevented penetration of 0.30 cal APM2 penetrators is shown in Figure 10. Tiles being completely pushed through the lattice structure indicated that aluminum lattice structures would need to be "backed up" with another layer of structure since the back face of the aluminum lattice structures are not strong enough for very high energy threats, such as 0.50 cal APM2 projectiles. An example of a SiC reinforcing tile pushed completely through an aluminum lattice structure is shown in Figure 11. Table 14 summarizes the penetration resistance performance for aluminum lattice castings.

Figure 10. An Al lattice structure with SiC tiles that stopped 0.30 cal APM2 penetrators; 8 mm thick SiC tiles stopped 0.30 cal APM2 penetrators at up to 2669 fps and 6 mm thick SiC tiles stopped 0.30 cal APM2 penetrators at up to 2426 fps.

Figure 11. Two SiC reinforcing tiles were pushed completely through an aluminum lattice structure by a 0.50 cal APM2 projectile.

Using the data from Table 14, models to predict the penetration resistance of aluminum lattice castings with embedded ceramic or hard metals tiles were developed. These models included erosion/deletion strain sets for each material and utilized the Johnson-Holmquist ceramic damage model that uses non-linear static and dynamic loading. The mesh size was optimized to ensure that the results were accurate and the computational time was minimized. The predicted values for residual velocity for A356 aluminum alloy lattice castings with no tiles being penetrated with 0.30 caliber APM2 projectiles agreed within 3-3.5% of the experimental values over the entire range of strike velocity examined, Figure 12.

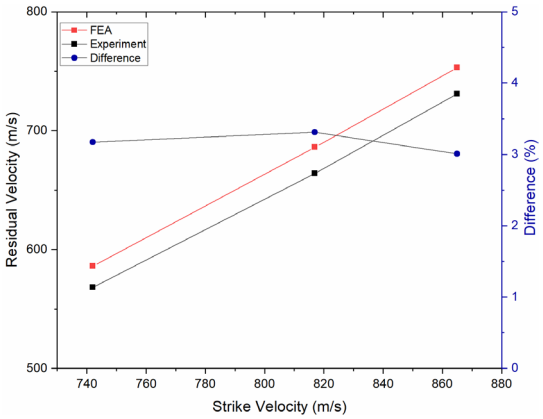

Figure 12. Residual velocity versus strike velocity for A356 aluminum alloy lattice castings with no tiles being penetrated with 0.30 caliber APM2 projectiles.

This model was then expanded to include the effects of a SiC tile. A residual velocity profile as a function of time is shown in Figure 13. For this model, the predicted values for residual velocity for A356 aluminum alloy lattice castings with 6 mm thick SiC tiles being penetrated with 0.30 caliber APM2 projectiles agreed within 2% of the experimental values.

Using the model for A356 aluminum alloy with a 6 mm thick SiC tile and a solid A356 aluminum alloy plate, a weight savings of 18% was predicted. A 62 mm thick, A356 aluminum alloy, lattice casting with 6 mm thick SiC tiles would have the same penetration resistance compared to 42.5 mm thick, solid, A356 aluminum alloy plate, Figure 14. The lattice casting would also be expected to absorb blast loads by compressing, whereas, the solid plate would transfer blast loads rather than absorb the blast energy.

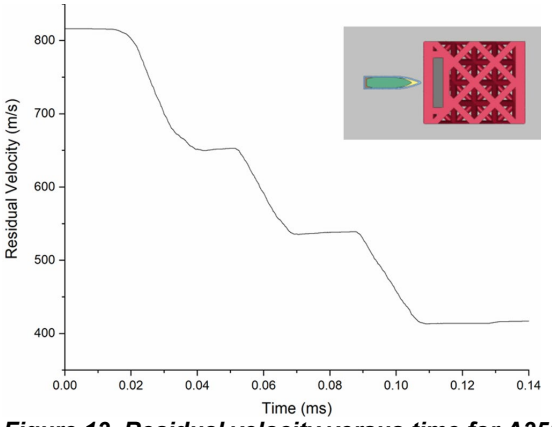

Figure 13. Residual velocity versus time for A356 aluminum alloy lattice castings with a 6 mm thick SiC tiles being penetrated with a 0.30 caliber APM2 projectile.

Table 14. Summary of Penetration Resistance Performance for Al Lattice Castings with 6 tiles (Tile location was behind the strike face).

Tile Material and Size	Threat	Strike Velocity (fps)	Residual Velocity (fps)	Velocity Reduction
none	7.62 x 51 mm, M80, ball round	2797	2159	23%
none	7.62 x 51 mm, M80, ball round	2838	1996	30%
4 mm thick SiC	7.62 x 51 mm, M80, ball round	2843	1057	63%
4 mm thick SiC	7.62 x 51 mm, M80, ball round	2470	not captured	
6 mm thick SiC	7.62 x 51 mm, M80, ball round	2843	0	no penetration
8 mm thick SiC	7.62 x 51 mm, M80, ball round	2807	0	no penetration
4 mm thick white cast iron	7.62 x 51 mm, M80, ball round	2821	0	no penetration
4 mm thick white cast iron	7.62 x 51 mm, M80, ball round	2998	870	71%
6 mm thick white cast iron	7.62 x 51 mm, M80, ball round	2808	0	no penetration
6 mm thick white cast iron	7.62 x 51 mm, M80, ball round	3016	0	no penetration
8 mm thick white cast iron	7.62 x 51 mm, M80, ball round	2822	0	no penetration
8 mm thick white cast iron	7.62 x 51 mm, M80, ball round	2995	0	no penetration
none	0.30 APM2	2436	1862	24%
none	0.30 APM2	2682	2178	19%
none	0.30 APM2	2837	2398	15%
none	0.30 APM2	3035	2777	9%
4 mm thick SiC	0.30 APM2	2887	2347	19%
4 mm thick SiC	0.30 APM2	2441	1237	49%
4 mm thick SiC	0.30 APM2	2343	1280	45%
6 mm thick SiC	0.30 APM2	2851	1858	35%
6 mm thick SiC	0.30 APM2	2678	1367	49%
6 mm thick SiC	0.30 APM2	2426	0	no penetration
8 mm thick SiC	0.30 APM2	2867	1168	59%
8 mm thick SiC	0.30 APM2	2669	0	no penetration
8 mm thick SiC	0.30 APM2	2462	0	no penetration
4 mm thick SiC	0.50 APM2	3051	2732	10%
8 mm thick SiC	0.50 APM2	3056	2702	12%

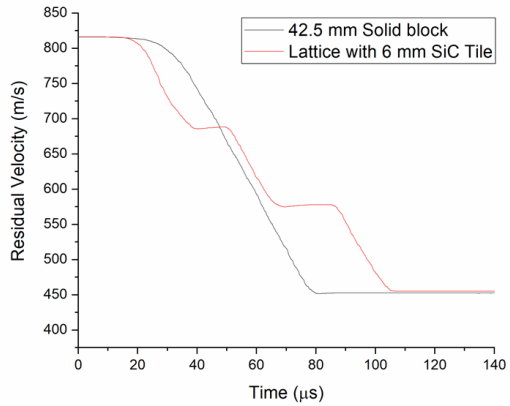

Figure 14. Comparison of residual velocity vs. time for a solid plate of A356 Al alloy and an A356 Al alloy lattice casting with 6 mm thick SiC tiles being penetrated with a 0.30 caliber APM2 projectile.

Additional refinements to this model included the effect of the strength of the interface between the tile and the cast metal on penetration resistance and the effect of tile residual stresses on penetration resistance. The effect of the strength of the interface on penetration resistance was small. Tile residual stresses, which would develop when the cast metal solidifies and shrinks, were predicted to decrease residual velocity by ~24%. The effect of the strength of the interface between the tile and the cast metal on penetration resistance is shown in Figure 15 and the effect of tile residual stresses on penetration resistance is shown in Figure 16.

Penetration resistance testing of A206 aluminum alloy with 1% TiC nanoparticles and 6 mm thick B_4C/SiC composite ceramic tiles produced by Eck Industries, Manitowoc, WI showed better performance compared to A356 aluminum alloy with 6 mm thick SiC tiles. Table 15 summarizes the penetration resistance performance for A206 aluminum alloy with 1% TiC nanoparticles and 6 mm thick B_4C/SiC composite ceramic tiles produced by Eck Industries.

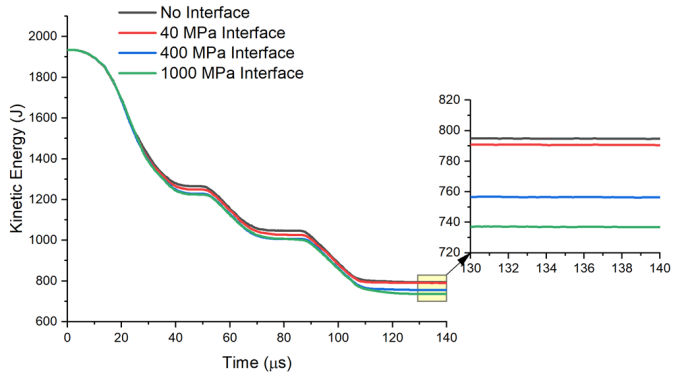

Figure 15. The effect of the strength of the interface between the tile and the cast metal on the penetration resistance of an A356 aluminum alloy lattice casting with 6 mm thick SiC tiles being penetrated with a 0.30 caliber APM2 projectile.

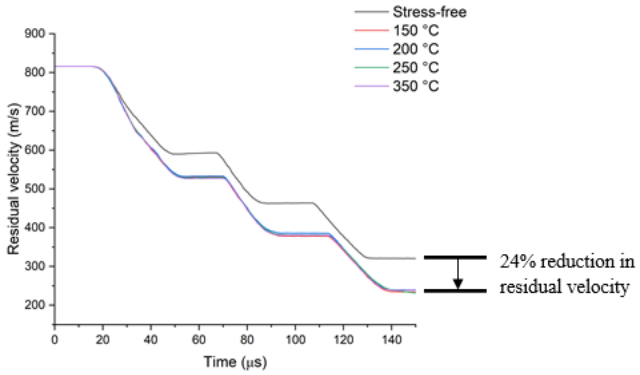

Figure 16. The effect of tile residual stresses on the penetration resistance of an A356 aluminum alloy lattice casting with 6 mm thick SiC tiles being penetrated with a 0.30 caliber APM2 projectile.

Table 15. Penetration Resistance of A206 Al Alloy with 1% TiC Nanoparticles and 6 mm Thick B_4C/SiC Composite Ceramic Tiles Produced by Eck Industries, Manitowoc, Wisconsin

Strike Location	Projectile	Strike Velocity (fps)	Penetration Results
Tile behind strike face	0.30 cal APM2	2815	Full penetration
Triple point between three tiles	0.30 cal APM2	2820	na**
Tile in front of back face	0.30 cal APM2	2829	Full penetration
Edges between two tiles	0.30 cal APM2	2822	na
Mid plane tile	0.30 cal APM2	2806	Full penetration
Tile behind strike face	0.30 cal APM2	2573	na
Triple point between three tiles	0.30 cal APM2	2892	na
Tile in front of back face	0.30 cal APM2	2615	Full penetration
Edges between two tiles	0.30 cal APM2	2904	Full penetration
Mid plane tile	0.30 cal APM2	2611	Full penetration
Tile behind strike face	0.50 cal FSP*	2705	na
Triple point between three tiles	0.50 cal FSP	2868	na
Tile in front of back face	0.50 cal FSP	3463	Full penetration
Edges between two tiles	0.50 cal FSP	3175	na
Tile behind strike face	0.50 cal FSP	3466	na

* FSP = fragment simulated projectile
** = Projectile did not completely penetrate

Penetration resistance testing of 15N20, quenched and tempered, high hardness, steel alloy lattice castings with integrally cast, 6 mm thick, 15N20 steel tiles showed much better performance compared to the aluminum alloy castings but this casting weighed significantly more. This casting weighed 27.9 lbs and was quenched and tempered to a hardness of 54 HRC. Table 16 summarizes the penetration resistance performance for 15N20 lattice castings with integrally cast, 6 mm thick, 15N20 steel tiles. A residual velocity of “na” indicates that the projectile did not completely penetrate.

Table 16. Penetration Resistance of 15N20 Quenched & Tempered Steel Alloy Lattice Castings with Integrally Cast, 6 mm thick, 15N20 Steel Tiles

Strike Location	Projectile	Strike Velocity (fps)	Residual Velocity (fps)
Tile behind strike face	0.30 cal APM2	3220	na**
Tile in front of back face	0.30 cal APM2	3241	na
Edges between two tiles	0.30 cal APM2	3249	na
Triple point between three tiles	0.30 cal APM2	3215	na
Tile behind strike face	0.50 cal FSP*	2328	na
Tile in front of back face	0.50 cal FSP	2438	na
Edges between two tiles	0.50 cal FSP	2445	na
Triple point between three tiles	0.50 cal FSP	2434	na
Tile behind strike face	20 mm FSP	2584	na

* FSP = Fragment simulated projectile
** = Projectile did not completely penetrate

Penetration resistance testing of 4365 quenched and tempered, ultra-high hardness, steel alloy lattice casting with integrally cast, 6 mm thick, 4365 steel tiles showed much better performance compared to the aluminum alloy castings but this casting also weighed significantly more. This casting weighed 25.7 lbs and was quenched and tempered to a hardness of 57 HRC (601 BHN). Table 17 summarizes the penetration resistance performance for the 4365 quenched and tempered, ultra-high hardness, steel alloy lattice casting with integrally cast, 6 mm thick, 4365 steel tiles. A residual velocity of “na” indicates that the projectile did not completely penetrate. This casting experienced catastrophic failure after five hits due to a lack of ductility.

Table 17. Penetration Resistance of 4365 Quenched & Tempered, Ultra-high Hardness, Steel Alloy Lattice Casting with Integrally Cast, 6 mm Thick, 4365 Steel Tiles

Strike Location	Projectile	Strike Velocity (fps)	Residual Velocity (fps)
tile behind strike face	0.50 cal FSP*	5203	na**
triple point between three tiles	0.50 cal FSP	5234	na
tile in front of back face	0.50 cal FSP	5241	full penetration
edges between two tiles	0.50 cal FSP	5251	na
mid plane tile	0.50 cal FSP	5231	catastrophic casting failure

* FSP = Fragment simulated projectile
** = Projectile did not completely penetrate

Penetration resistance testing of Fe30Mn4Al1Si0.9C as-cast steel alloy lattice castings with 6 mm thick, white cast iron tiles also showed much better performance compared to the aluminum alloy castings but, again, this casting weighed significantly more. These castings had an areal density of about 45 lbs/sq ft. Table 18 summarizes the penetration resistance performance for an Fe30Mn4Al1Si0.9C as-cast steel alloy lattice casting projectile, 0.50 cal fragment simulated projectiles, and 20 mm fragment simulated projectiles. The strike velocity to achieve complete penetration of an Fe30Mn4Al1Si0.9C as-cast steel alloy lattice casting with 6 mm thick, white cast iron tiles using 0.50 cal or 20 mm fragment simulated projectiles has not yet been determined. A residual velocity of "na" indicates that the projectile did not completely penetrate.

Table 18. Penetration Resistance of Fe30Mn4Al1Si0.9C As-cast Steel Alloy Lattice Casting with 6 mm Thick, White Cast Iron Tiles

Strike Location	Projectile	Strike Velocity (fps)	Residual Velocity (fps)
Tile behind strike face	0.30 cal APM2	2831	na*
Tile behind strike face	0.30 cal APM2	3200	706
Tile in front of back face	0.30 cal APM2	3161	na
Edges between two tiles	0.30 cal APM2	3192	na
Triple point between three tiles	0.30 cal APM2	3168	na
Tile behind strike face	0.50 cal FSP**	6898	na
Tile in the middle of the casting	0.50 cal FSP	6933	na
Tile in front of back face	0.50 cal FSP	6920	na
Tile behind strike face	20 mm FSP	3449	na
Tile in the middle of the casting	20 mm FSP	3531	na
Tile in front of back face	20 mm FSP	3508	na

* = Projectile did not completely penetrate, no damage to witness plate
** FSP = Fragment simulated projectile

INDUSTRY VERIFICATION

Eck Industries produced 225 mm x 225 mm x 62 mm lattice castings with 4 mm diameter trusses in A206 aluminum alloy with 1% TiC nanoparticles with and without tiles. These castings did not hot tear and were heat treated to the T4 temper. Two castings successfully poured at Eck Industries are shown in Figure 18.

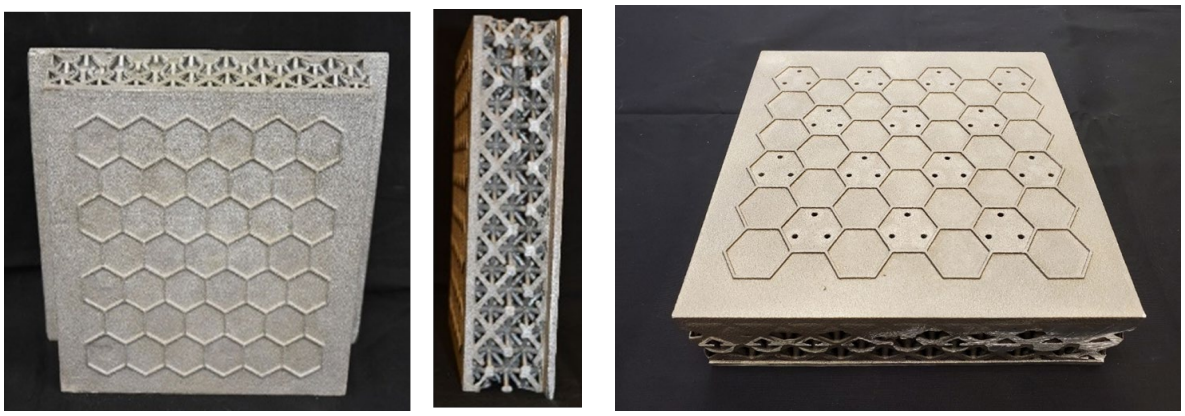

A206 casting with no tiles A206 casting with 39 B_4C/SiC tiles

Figure 18. Two, 225 mm x 225 mm x 62 mm lattice castings with 4 mm diameter trusses successfully poured at Eck Industries in A206 aluminum alloy with 1% TiC nanoparticles.

Trident Alloys poured 225 mm x 225 mm x 62 mm lattice castings in 4365 alloy steel. Unfortunately, one casting had an incomplete fill due to low pouring temperature and another casting had core float due to core supports that broke during shipping of the mold. The 4365 alloy steel that had core float is shown in Figure 19.

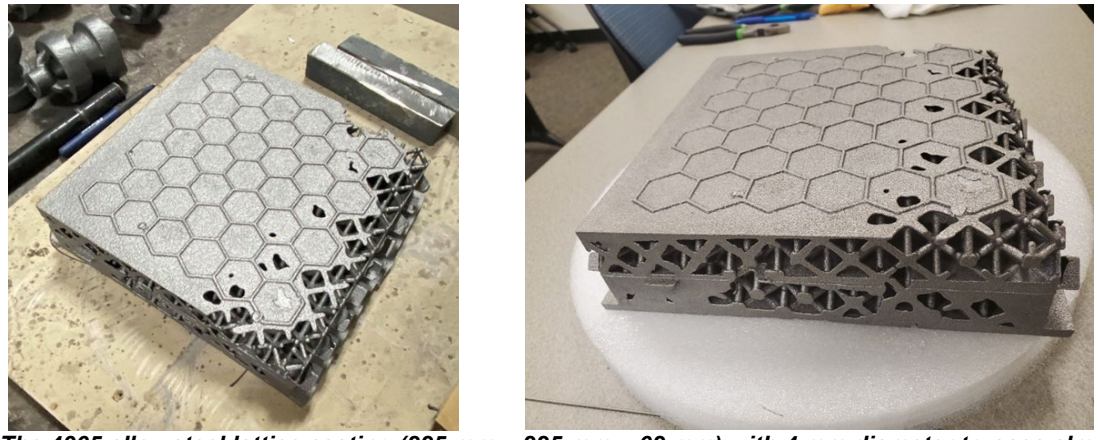

Figure 19. The 4365 alloy steel lattice casting (225 mm x 225 mm x 62 mm) with 4 mm diameter trusses almost successfully poured at Trident Alloys. The core floated due to core supports that broke during shipping of the mold.

SUMMARY

Complex lattice castings can be produced using 3D printed sand molding. Further, lattice castings with embedded ceramic or hard metal tiles were produced using 3D printed sand molding. Investment casting could be used to produce lattice castings with no embedded tiles but there are no casting or additive manufacturing processes that can produce a lattice casting with embedded tiles.

As expected, alloy steel lattice castings had better penetration resistance compared to aluminum alloy lattice castings but alloy steel castings were significantly heavier. The combination of Fe30Mn4Al1Si0.9C steel alloy with 6 mm thick, white cast iron tiles had the best overall penetration resistance. The areal density of Fe30Mn4Al1Si0.9C steel alloy with 6 mm thick, white cast iron tiles is estimated at 45 lbs/sq ft. The Fe30Mn4Al1Si0.9C steel alloy has reasonable high yield strength and very high ductility while white cast iron has reasonably high hardness and better fracture toughness compared to the ceramics evaluated. Fe30Mn4Al1Si0.9C steel alloy with 6 mm thick, white cast iron tiles stopped 0.30 cal APM2 penetrators at the maximum velocity obtainable (~3200 fps), stopped 0.50 cal fragment simulated projectiles at velocities up to 6933 fps, which is equivalent to a projectile energy of 29,919 Joules, and stopped 20 mm fragment simulated projectiles at velocities up to 3531 fps, which is equivalent to a projectile energy of 31,159 Joules

To date, the largest lattice castings produced have been 335 mm x 335 mm x 62 mm with no tiles or with one hundred five, 6 mm thick, SiC tiles, Figure 20. These castings were produced in A356 aluminum alloy with gravity pouring. To produce larger castings, vacuum riserless or low-pressure casting processes will be necessary.

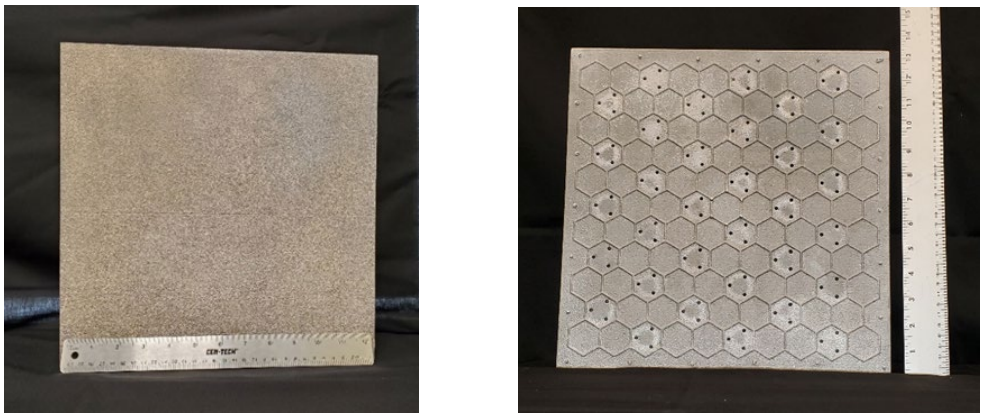

no tiles with 105 SiC tiles

Figure 20. The largest lattice castings produced were 335 mm x 335 mm x 62 mm with no tiles or with one hundred five, 6 mm thick, SiC tiles in A356 aluminum alloy using gravity pouring.

Models were developed using commercially available software that accurately predicted the penetration resistance of A356 aluminum alloy castings with and without SiC tiles. Using these models, a weight savings of 18% was predicted for a lattice casting with 6 mm thick SiC tiles compared to a solid plate of A356 alloy. The lattice casting would also be expected to absorb blast loads by compressing, whereas, the solid plate would transfer blast loads rather than absorb the blast energy. The penetration resistance models were expanded to include the effects of the strength of the interface between the ceramic tile and the cast metal and the effect of tile residual stresses.

Models were also developed using commercially available software to predict the slow strain rate performance of a variety of lattice unit cells, such as the octet truss, auxetic truss, Kelvin foam, circular octet, and face centered truss. The auxetic truss was predicted to have the best performance but was also one of the most difficult to produce. The octet truss was predicted to have the best combination of performance and manufacturability. These models can be used by designers to develop lattice structure that will have the required properties for a given application.

The thermophysical properties of Fe30Mn4Al1Si0.9C steel were predicted using a commercially available computational materials engineering software package, and these properties were used to create a database for mold filling and solidification. This database was provided to the US Army FeMnAl working group, presented at the *2021* International Materials, Applications & Technologies Conference, and published in the *International Journal of Metalcasting (IJMC)*.[21]

ACKNOWLEDGEMENTS

This research was sponsored by the Defense Logistics Agency Information Operations, J68, Research & Development Office, Ft. Belvoir, VA and the DLA Troop Support, Philadelphia, PA. The Virginia Tech project team would also like to thank the companies that provided in-kind support: MAGMAsoft, ExOne, Systems Engineering & Manufacturing, Eck Industries, Danko Arlington, Trident Alloys, BRP, and North Star Imaging. The Virginia Tech project team would also like to acknowledge NTS Chesapeake for penetration testing services, Oak Ridge National Lab for access to neutron imaging and neutron diffraction at the High Flux Isotope Reactor, Argonne National Lab for access to synchrotron diffraction, and Humtown for making 3D printed molds.

REFERENCES

1. L.J. Gibson and M.F. Ashby, “Cellular Solids: Structure and Properties,” 2nd ed. (Cambridge Solid State Science Series), Cambridge University Press (1997).
2. M.F. Ashby, "The properties of foams and lattices," *Philos Trans A: Math Phys Eng Sci*, vol. 364, no. 1838, pp. 15-30(Jan 15, 2006). https://doi.org/10.1098/rsta.2005.1678
3. J. Banhart and D. Weaire, "On the Road Again: Metal Foams Find Favor," *Physics Today*, vol. 55, no. 7, pp. 37-42 (2002). doi: 10.1063/1.1506749
4. V.S. Deshpande, M.F. Ashby, and N.A. Fleck, "Foam topology: bending versus stretching dominated architectures," *Acta Materialia*, vol. 49, no. 6, pp. 1035-1040, 2001/04/02/ (2001). https://doi.org/10.1016/S1359-6454(00)00379-7 (Link last accessed 04-04-24.)
5. M. Leary *et al.*, "Inconel 625 lattice structures manufactured by selective laser melting (SLM): Mechanical properties, deformation and failure modes," *Materials & Design,* vol. 157, pp. 179-199 (2018) 11/05/ 2018. h t t p s ://doi.org/10.1016/j.matdes.2018.06.010 (Link last accessed 04-04-24.)

6. R. Mahshid, H. N. Hansen, and K. L. Højbjerre, "Strength analysis and modeling of cellular lattice structures manufactured using selective laser melting for tooling applications," *Materials & Design,* vol. 104, pp. 276-283, 2016/08/15/(2016). doi: https://doi.org/10.1016/j.matdes.2016.05.020 (Link last accessed 04-04-24.)
7. R. Voillat, F. Gallien, A. Mortensen, and V. Gass, "Hypervelocity impact testing on stochastic and structured open porosity cast Al-Si cellular structures for space applications," *International Journal of Impact Engineering,* vol. 120, pp. 126-137, 2018/10/01/ (2018). doi: https://doi.org/10.1016/j.ijimpeng.2018.05.002 (Link last accessed 04-04-24.)
8. V.H. Carneiro, S.D. Rawson, H. Puga, J. Meireles, and P. J. Withers, "Additive manufacturing assisted investment casting: A low-cost method to fabricate periodic metallic cellular lattices," *Additive Manufacturing,* vol. 33, p. 101085, 2020/05/01/ (2020). doi: https://doi.org/10.1016/j.addma.2020.101085 (Link last accessed 04-04-24.)
9. D.A. Snelling, C.B. Williams, and A.P. Druschitz, "Mechanical and material properties of castings produced via 3D printed molds," *Additive Manufacturing,* vol. 27, pp. 199-207, 2019/05/01/ (2019). doi: https://doi.org/10.1016/j.addma.2019.03.004 (Link last accessed 04-04-24.)
10. C.R. Hasbrouck, J.W. Fisher, M.R. Villalpando, and P.C. Lynch, "A Comparative Study of Dimensional Tolerancing Capabilities and Microstructure Formation between Binder Jet Additively Manufactured Sand Molds and Olivine Green Sand Molds for Metalcasting of A356.0," *Procedia Manufacturing,* vol. 48, pp. 338-348, 2020/01/01/ (2020). doi: https://doi.org/10.1016/j.promfg.2020.05.056 (Link last accessed 04-04-24.)
11. A. Druschitz *et al.*, "Metal-Ceramic composite lattice structures using 3D printed sand molds and cores," in *2016 International Solid Freeform Fabrication Symposium*, 2016: University of Texas at Austin (2016).
12. D.A. Snelling, Jr., "A Process for Manufacturing Metal-Ceramic Cellular Materials with Designed Mesostructure," PhD Dissertation (2015). https://ui.adsabs.harvard.edu/abs/2015PhDT.....581S (Link last accessed 04-04-24.)
13. D. Ashouri *et al.*, "Mechanical behaviour of additive manufactured 316L f2ccz lattice structure under static and cyclic loading," *International Journal of Fatigue,* vol. 134, p. 105503, 2020/05/01/ (2020). https://doi.org/10.1016/j.ijfatigue.2020.105503 (Link last accessed 04-04-24.)
14. S. Das, D. L. Bourell, and S. S. Babu, "Metallic materials for 3D printing," *MRS Bulletin,* vol. 41, no. 10, pp. 729-741 (2016). https://doi.org/10.1557/mrs.2016.217 (Link last accessed 04-04-24.)
15. J.H. Martin, B.D. Yahata, J.M. Hundley, J.A. Mayer, T.A. Schaedler, and T.M. Pollock,"3D printing of high-strength aluminium alloys," *Nature,* 549, 365–369 (2017). https://doi.org/10.1038/nature23894 (Link last accessed 04-04-24.)
16. "Designations and Chemical Composition Limits for Aluminum Alloys in the Form of Castings and Ingot," The Aluminum Association, Inc., Arlington, VA (2015).
17. Chesapeake Testing, A Division of NTS, https://nts.com/location/belcamp-md/ (Link last accessed 04-04-24.)
18. Ansys LS-DYNA, Multiphysics Solver, https://www.ansys.com/products/structures/ansys-ls-dyna (Link last accessed 04-04-24.)
19. MAGMASOFT, https://www.magmasoft.com/en/ (Link last accessed 04-04-24.)
20. Thermo-Calc, https://thermocalc.com/ (Link last accessed 04-04-24.)
21. M. Umanzor, M. Drew, A. Druschitz, "Thermophysical Properties of Fe30Mn4Al0.9C: A Coupled Computational-Experimental Approach," *International Journal of Metalcasting*, 16, 521-534 (2022). doi: https://doi.org/10.1007/s40962-021-00624-5 (Link last accessed 04-04-24.)